Fabrication, Characterization of locally strained 2D Heterostructure

Chenfeng Du

A dissertation

submitted in partial fulfillment of the

requirements for the degree of

Master of Science in Materials Science and Engineering

University of Washington

2023

Reading Committee:

Xiaodong Xu, Chair

Ting Cao

Program Authorized to Offer Degree:

Materials Science and Engineering

University of Washington

Abstract

Fabrication, Characterization of locally strained 2D Heterostructure

Chenfeng Du

Chair of the Supervisory Committee:
Professor Xiaodong Xu
Professor of Department of Physics and Materials Science and Engineering，
Adjunct Professor of Electrical and Computer Engineering

Two-dimensional materials are atomic thick when exfoliated down to monolayers. 2D semiconductors are of special interests because they have a bandgap that graphene does not，hence they provide a good platform for studying physics and future devices. 2D semiconductors， especially monolayer of WSe2 and MoSe2, have a series of advantages, including light-matter interaction, excitons, and valleys. The abundant spectra information also enables the potentially applications in solar energy capture. With current in-lab fabrication techniques, researchers are able to fabricate heterostructures by precisely restacking different sheets into van der Waals force bound stack. The combination of self-designed heterostructures enables further study on emerging phenomenon and novel physics. Researchers are familiar with manipulating these heterostructures using electrical, magnetic, pressure and mechanical methods to study the abundant exciton physics. However, one extra degree of freedom, strain, remains poorly understood. The strain in bulk transition metal dichalcogenides (TMDS) is usually introduced during crystal growth. Once exfoliated, there is less confinement from both the upper and lower layers. Therefore, strain inherited from interfacial contact gives the heterostructure an

complicated out-of-plane degree of freedom. Because the 2D material has a tensile feature and endures considerable stress and compression, the interface between the heterostructure and substrate becomes a dominant factor that affects the strain in heterostructure. In my thesis, substrate with different surface topographies is applied. Firstly, I placed the heterostructure of WSe2/MoSe2 on nano-diamond to introduce strain in the materials. To make the strain more controllable, one or two layers WSe2 was fixed on the top of pillars. With optical characterization combined, both energy shifts and fine features in photoluminescence are observed in different materials. These sample preparation experiments mark the first step towards more extensive related research.

TABLE OF CONTENTS

Science and technology are going into smaller and smaller scale, from bulk materials to atomic-scale structure. Starting in 2004 when graphene was first isolated using “peel off” method in the lab [1], more and more 2D atomic crystals then were well-researched [2] and even brought to realistic applications. Over the past twenty years, kinds of technology have been developed quickly to explore the features of materials at nanoscale, such as the atomic force microscopy, scanning tunneling microscopy, and optical Kerr microscopy.

As shown of the roadmap in Figure 1, with 2D atomic crystal family showing up in the spotlight, there has been accelerating and fast evolving progress from two-dimensional device to applications [3][4][5][6][7][8][9][10][11][12][13][14][15][16]. Among the abundant 2D materials family, the two-dimensional semiconductor research has been experiencing an accelerating frontier starting in 2005, when researchers first managed to isolate a two-dimensional semiconductor from bulk materials with micromechanical cleavage [2]. Another milestone was realized in 2013, there was a leap from monolayer to stack, where researchers managed to stack the different materials in a precisely chosen sequence to form van der Waals interaction bound heterostructures [17][18]. This fabrication technology contributes to the fast-evolving process in condensed matter physics researches by enabling the fabrication of 2D electronic, photonic, and optoelectronic devices [19].

The two-dimensional material has unique textile feature and can undergo bending, wrinkling, and some stretching. This allows us to tune and change its physical property and to develop new applications.

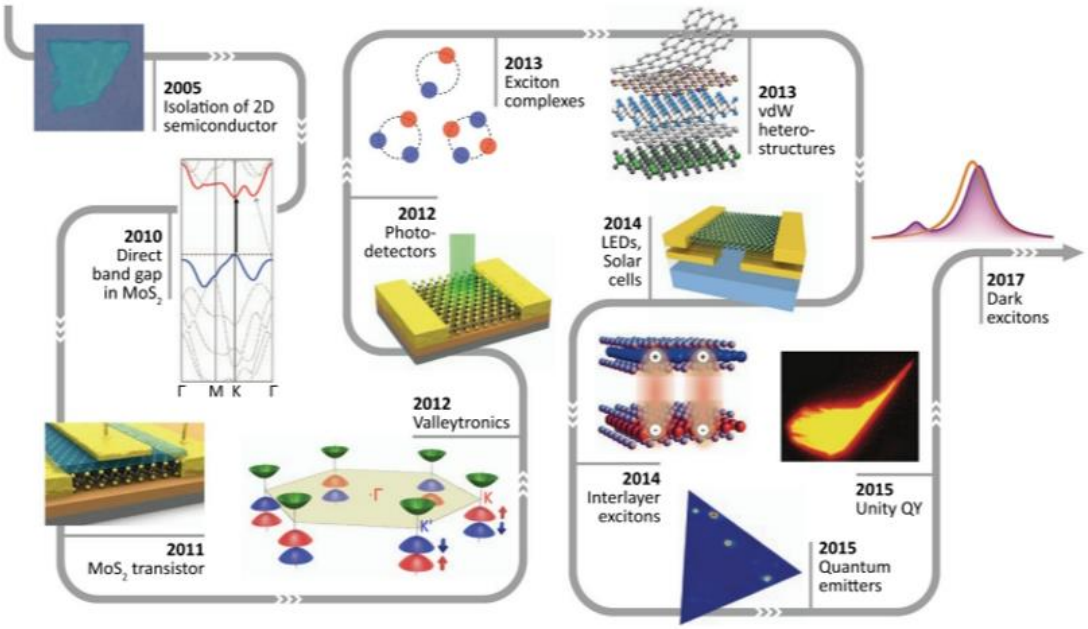

Figure 1. The roadmap of two-dimensional semiconductor research progress[36]

In perfect bulk crystal, strain is usually too small to affect the material's properties. Different from the bulk materials, the strain in two dimensional materials is ubiquitous and leads to abundant properties, which can be tuned to change the physical property and develop new applications. Besides the naturally occurring, tactile deformation, piezoelectric substrates, and viscoelastic substrates are the common methods to actively tune strain of 2D materials [20][21], as shown in Figure 2. Instead of the traditional strain engineering methods listed above, here we introduce and engineer the strain via substrate indentation, which means the surface topography on the substrate is shaped. There are two ways to be employed, nano particles and pillar substrate, shown in Figure 3.

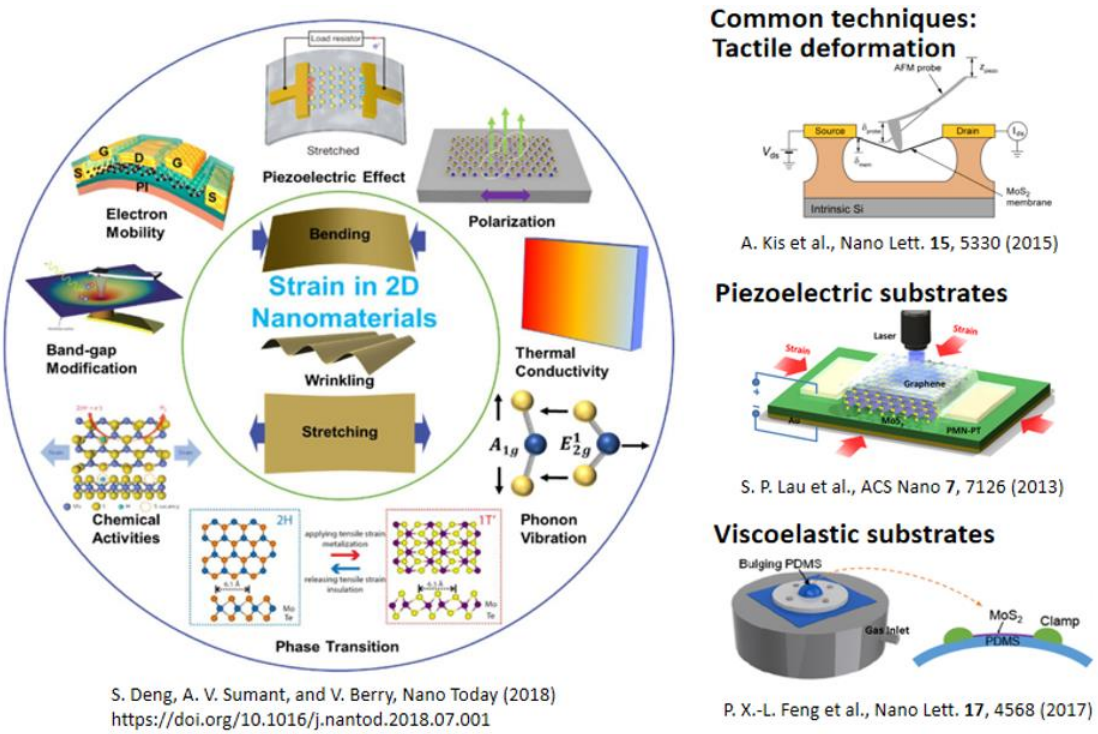

Figure 2. Strain in 2D nanomaterials [21]

2-dimensional material are usually atomic thick and has an inherited out-of-plane freedom compared to their 3-dimensioanl bulk crystals. This unique textile feature allows us to tune and change the physical property and to develop new applications of two-dimensional materials. The strain in two-dimensional material is ubiquitous and lead to abundant properties, traditional common techniques include: tactile deformation [22], piezoelectric substrates [23] and viscoelastic substrates [24].

The transition metal dichalcogenides have a direct bandgap when isolated and therefore is getting more consideration [25]. In our lab, there have been many researches published based on WSe_2 and $MoSe_2$. As part of the transition metal dichalcogenides (TMDs), WSe_2 and $MoSe_2$ have properties that complement those of graphene. Similar to graphene, TMD have a layered structure bound by weak van der Waals force, and thus bulk crystals are easily reduced to ultrathin thickness, allowing monolayer extraction by mechanical exfoliation with scotch tape.

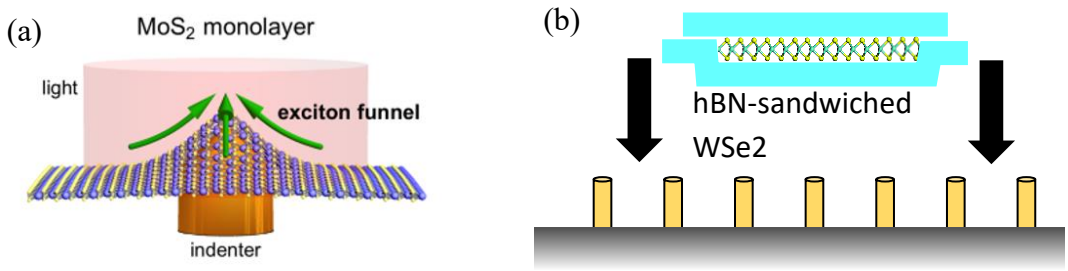

Figure 3. By shaping the surface topography, we introduce strain via substrate indentation. Both (a) nanoparticles and (b) nanopillars are employed to change the strain.

Here, my research focus on fabrication and characterization of locally strain-tuned WSe2 and MoS_2 and the heterostructure. I firstly prepared the 2D samples by peel-off method. Then a home-built micromanipulator is used to precisely transfer the 2D samples to the substrate with nanoparticles and nanopillars on it to increase the strain. With optical characterization combined, both energy shift and fine feature in photoluminescence is observed in different materials.

Chapter 2: Heterostructure of WSe2/MoSe2 on nano-diamond

In this chapter, I use nanodiamond to create strain in WSe_2 / $MoSe_2$, to control the electronic and optical properties. Both of $MoSe_2$ and $MoSe_2/WSe_2$ are encapsulated in h-BN and have been indented on nanodiamond, respectively. Unlike in most heterostructures where h-BN serves only as an ultra-flat substrate [26][27], the h-BN here serve as protection layers that prevents the middle TMD from piercing. The strain induced properties have been observed with optical spectrum.

2.1 h-BN encapsulated 1L MoSe2 on nano-diamond

In 2010, Heinz and Wang independently demonstrated that monolayer molybdenum disulfide exhibits a direct bandgap and strong photoluminescence[28][29]. This occurs when bulk molybdenum disulfide material is exfoliated and thinned down to a monolayer, causing a change in bandgap from indirect to direct and a strong interaction between light and the material. This phenomenon has been widely observed in two-dimensional semiconductors MX_2 (M= W, Mo, X= S, Se). Since then, subsequent research has used photoluminescence on molybdenum disulfide material to investigate the effect of strain on optical and electronic properties, particularly in relation to textile deformations, piezoelectric substrates, and viscoelastic substrates.

Strain has emerged as a pivotal research topic in relevant fields. Moreover, strain in two-

dimensional materials has been found to be pervasive, resulting in a wide range of properties detailed in the literature. The high stretchability and controllable manipulation of the optical and electronic properties make the new families of two-dimensional crystals a fascinating subject of study. Strain engineering, which explores how the physical properties of materials can be adjusted by controlling the elastic strain fields exerted on them, finds an ideal application in atomically thin semiconducting materials[30][31]. Therefore, effectively controlling strain in two-dimensional materials and employing strain engineering holds great promise for manipulating the optoelectronic properties of semiconductors like tungsten diselenide and molybdenum diselenide.

In this chapter, we utilize nanodiamonds to induce strain in WSe_2 / $MoSe_2$ and manipulate their electronic and optical properties. The $MoSe_2$ and $MoSe_2/WSe_2$ structures are encapsulated in h-BN and then attached to the nanodiamond, allowing for the preparation and characterization of localized excitons-controlled by strain in WSe_2, $MoSe_2$, and their heterostructures. By applying external strain using the nanodiamond, we observe changes in the material properties through spectroscopy.

The inspiration for this concept stems from a prior study in 2016, where researchers recognized the potential of non-uniform strain distribution for creating exciton funnels[32]. This phenomenon enables excitons to migrate outwards from the strain gradient of black phosphorus or concentrate in the strain gradient center of MoS_2 (Figure 4). As a result, this technique can capture a broad range of solar spectra and concentrate carriers within a confined region of the

sample.

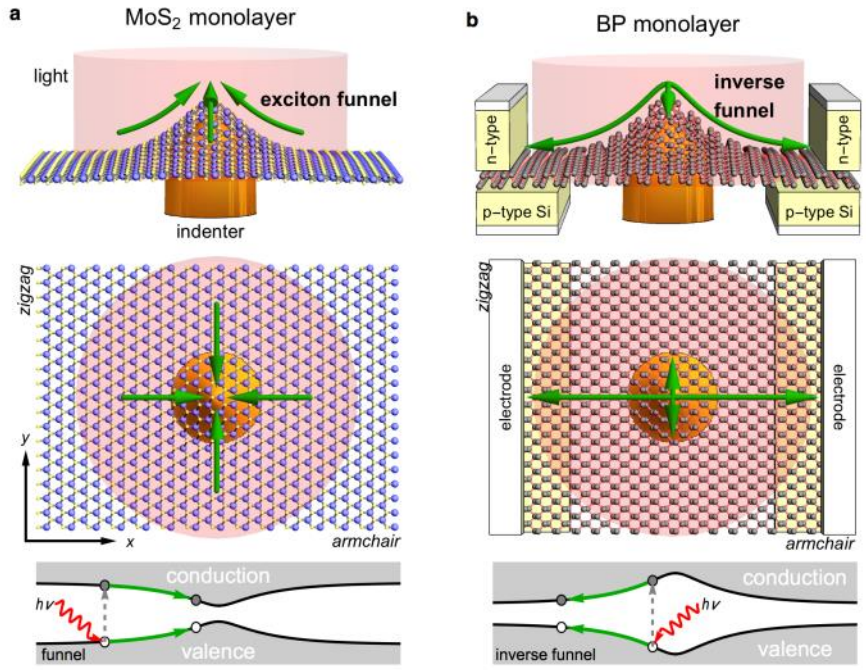

Figure 4. Strained induced funnel effect of excitons in 2D crystals. An indenter creates an inhomogeneous profile of strain in single layer MoS_2 (a) and black phosphorene (b). The strain gradient modulates the gap of the two crystals as sketched in the bottom panel. Photogenerated excitons (green arrows) are pushed isotropically towards the indenter center in MoS_2 (funnel effect), while they are pushed anisotropically away it in black phosphorus (inverse funnel effect). Adapted from Ref. 33 with permission of the American Physical Society.

To reproduce the effects of substrate-like indentations and create similar illustrations, we employ nanodiamonds to induce strain in tungsten diselenides and molybdenum diselenide. Our objective is to exert control over the electronic and optical properties of these materials. Figure 4 displays the heterostructure of molybdenum diselenide and tungsten diselenide, both encapsulated by hexagonal boron nitride layers.

In Figure 5(a), an image depicts nanodiamonds after spin-coating onto silicon oxide and silicon

substrates. Beneath the main image, scattered white and black dots are visible, representing the nanodiamonds used by the collaborators. Subsequent atomic force microscopy scanning (Figure 5(b)) reveals the presence of typical diamond shapes, with approximate lateral dimensions of two micrometers and heights ranging from 200 to 300 nanometers.

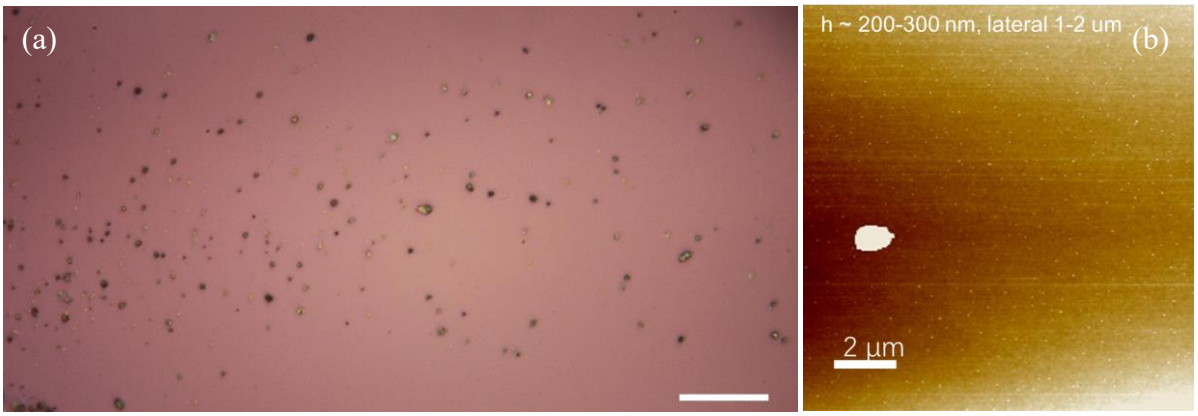

Figure 5. Nano-diamond on SiO_2/Si substrate (a) optical microscope image of nano diamond spin-coated onto substrate with scale bar of 100µm (b) atomic force microscope image of an isolated nano-diamond, lateral size is ~1µm*1.5µm, height is 200~300nm

For our experiment, a relatively isolated nanodiamond is carefully selected and used as a foundation to deposit a honeycomb-like structure, consisting of a $MoSe_2$ layer encapsulated with top and bottom hexagonal boron nitride layers (Figure 6). The optical microscope image on the Figure 6(a) showcases a substantial blue-green region, which corresponds to the top and bottom encapsulation layers of hexagonal boron nitride. Monolayer of $MoSe_2$ is encapsulated in between. The heterostructure stack is covered on top of a small isolated nanodiamond (Figure 6(b) and 6(c)). Interestingly, the presence of bubble-like formations with a rainbow-colored appearance is noticeable. These bubbles originate from the unevenness of the contact between

heterostructure and diamond spin-coated substrate surface. While the formation of bubbles is inevitable, we luckily managed to avoid their occurrence in the nanodiamond region. Finally,

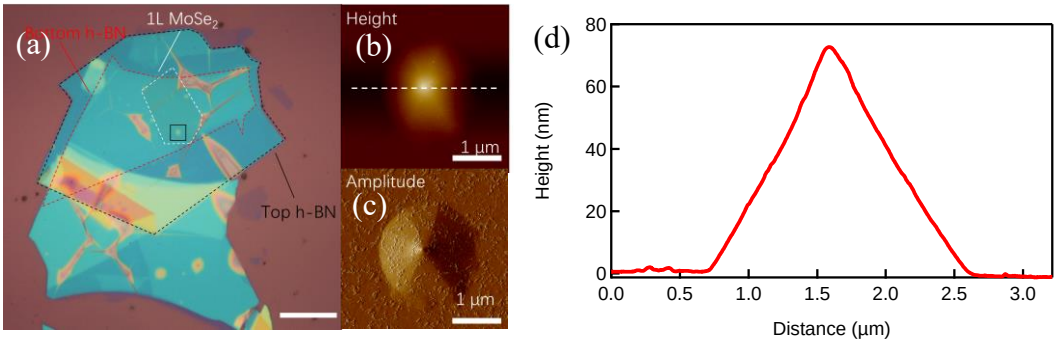

we conducted atomic force microscopy scanning on the nanodiamond.

Figure 6. (a) h-BN encapsulated monolayer $MoSe_2$ with nano-diamond substrate indentation (b)AFM height of nano-diamond underneath (c) AFM amplitude of nano-diamond underneath (d) cross-section on white dashed line in Fig. 6 (b) shows the uniform nanodiamond strain

The shape of the nanodiamond can be seen from Figure 6(d), revealing a height of approximately 65 nanometers below the nanodiamond and a lateral distribution of about two micrometers. We conducted preliminary tests on and off the nanodiamond, and the count rates are measured correspondingly. The plotted photoluminescence spectra in Figure 7(b) have been background-subtracted, providing three key observations. Firstly, when the distance from the nanodiamond is increased, indicating lower strain in the two-dimensional material, a stronger peak intensity can be observed, which represents the overall spectral characteristic. When positioned on the top of the nanodiamond, there is a significant decrease in the peak intensity of photoluminescence, accompanied by a blue shift in the peak energy, suggesting a shift towards the blue region. Additionally, the peak shape on the top surface of the nanodiamond undergoes deformation, indicating the presence of subtle structures. To further investigate, we

also examined molybdenum diselenide and tungsten diselenide encapsulated in hBN in Figure 8, which were deposited on an isolated nanodiamond.

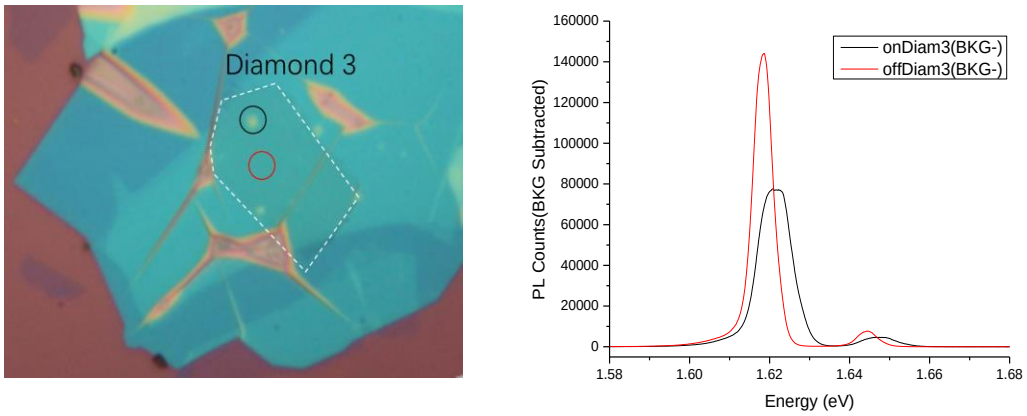

Figure 7. Optical characterization on/off nano-diamond strain. (a)zoom-in optical image of h-BN encapsulated monolayer $MoSe_2$ with nano-diamond indentation. $MoSe_2$ monolayer outlined with white-dashed line. Excitation spot with and without strain are indicated with **black** and **red** circles separately. (b) PL characterization of sample with/without nano-diamond indentation. PL intensity drops on diamond top, accompanied with energy blue shift.

Usually under tensile strain, the monolayer $MoSe_2$ exhibits energy red shift, however, here it exhibits energy blue shift, and this might come from the complicated diamond indentation induced strain and the huge bubble and crack around the sample that also introduces strain into the sample through encapsulating thick h-BN layers. The dielectric environment's influence on sample is critical to the these 2D atomic crystals, as they may affect the band structure and therefore tune the exciton properties [33].

The molybdenum diselenide is indicated by black dots, while the WSe_2 is indicated by red dots. The nanodiamond of interest is positioned at the edge of this curve, resulting in the formation of a sizable air bubble during the preparation process. Additionally, other bubbles can be observed outside the region of the heterostructure, and the generation of nanobubbles in this

area is unavoidable. The shape of the sample, where our heterostructure is situated, is delineated in this optical microscope image.

2.2 h-BN encapsulated $WSe_2/MoSe_2$ heterobilayers on nano-diamond

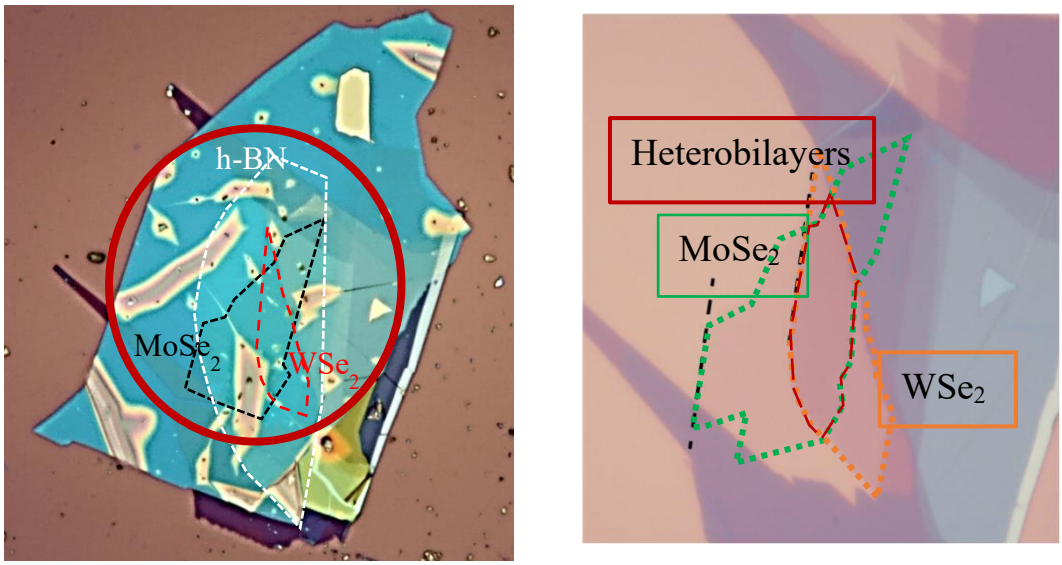

Figure 8. h-BN encapsulated $MoSe_2/WSe_2$ heterobilayers with nano-diamond indentation. (a) The left picture. Optical microscope image of sample. irregular shapes on the sample are bubbles formed during fabrication process. Black particles are nano-diamond on substrate. Bubble usually appear when there is rough contact interface between 2-dimensional sample and substrate, here we see the bubbles appear in sample when there is close proximity to more than one nano-diamond underneath. Outlined is the heterobilayer region. Detailed information see (b). (b) The right picture. Optical microscope image of sample, this is before depositing onto substrate, which is an easier way to look at the heterobilayer and the stack of $MoSe_2$ and WSe_2.

So, similar to our previous approach, we aimed to investigate the influence of strain under nanodiamond on the photoluminescence of two-dimensional materials. Figure 9 illustrates the heterostructure diagram, providing crucial information. Firstly, the photoluminescence of the interlayer exciton appears to emanate from the top of a large bubble located in the lower-left

corner of the heterostructure. As previously mentioned, this prominent bubble is situated within the sample's heterostructure. The photoluminescence of the heterostructure is observed on both the enormous bubbles in the lower-left corner and the edges. This shape is consistent with the sample design in this region.

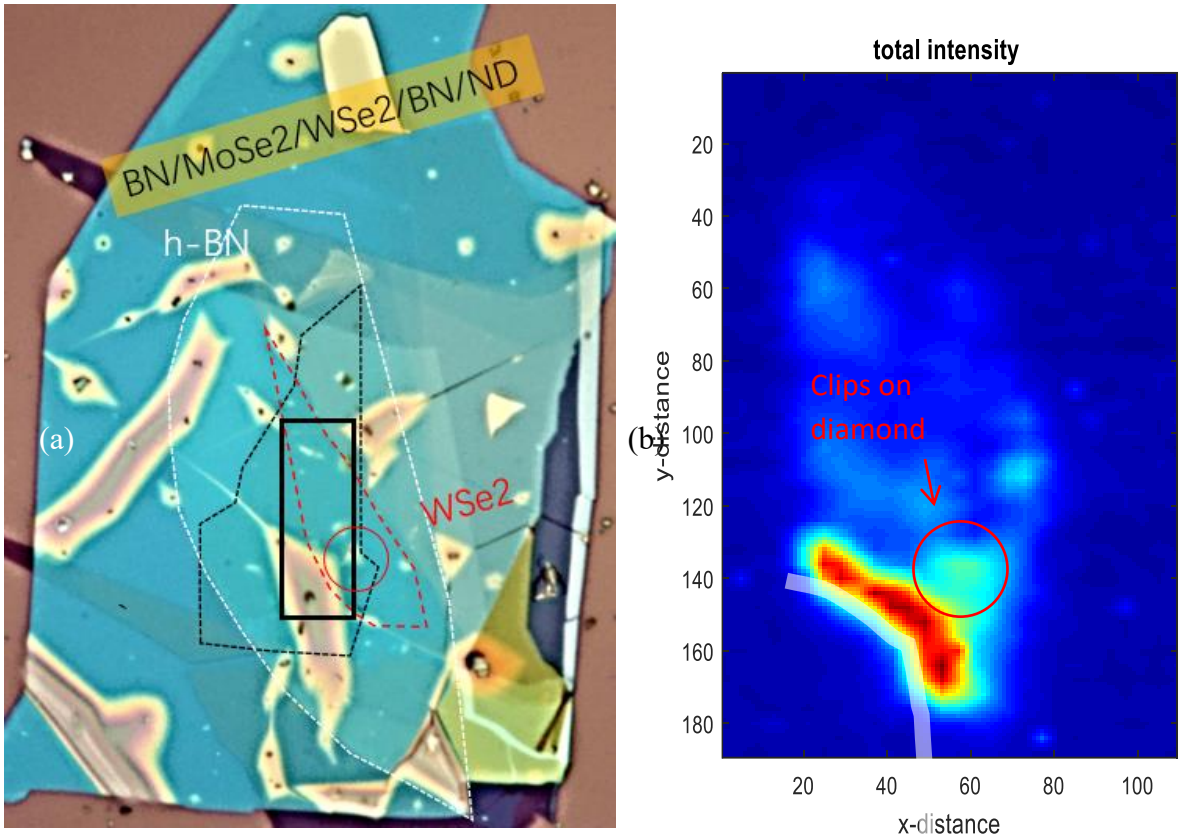

Figure 9. PL scanning map of heterobilayer of rectangle region. (a) Outlined region of heterobilayer , 1L MoSe2 and 1L WSe2. The left bottom of heterostructure clips on bubble edge and the diamond is on the right bottom egde, next to the bubble.

A motor stage with micro step is used to scan the rectangle area and PL collected is plotted in Figure 9(b). Figure 9(b) the scanning PL 2D map of heterobilayer. Position and PL brightness

is plotted in this 2D map. By comparing to the optical image of sample shape, we can see the bright higher PL intensity is seen when on nano-diamond and on bubble edge. This directly indicates that local strain from bubble/diamond enhances PL intensity. Nano-diamond and bubble edge of sample is highlighted in Figure 9 (a) for graph reading.

In this particular area, we observe the edge of a large bubble. The diamond adjacent to the bubble, visible in this optical image, is located in close proximity. It can be identified as the

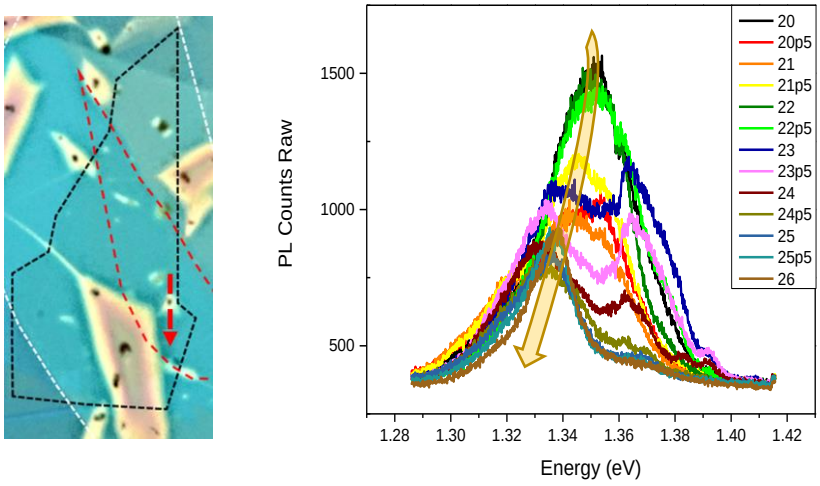

circular-shaped feature. While this does result in a slight increase in PL, it is not as significant as the enhancement observed in the huge bubble. Additionally, we conducted a manual exploration of the unstrained region and did not identify any other regions with extremely strong PL.

Figure 10. Position dependence PL of hetero bilayer. This is a series PL of different spot across the nanodiamond. (a) spot trajectory is depicted with red-dashed arrow, with 0.5μm step spacing. (b) By comparing the PLs to optical image in (a), we see the PL undergoes intensity increase when approaching the nano-diamond. When on diamond top, the PL intensity drops and shows split peak feature. When the position moves off diamond and towards bubble, the split PL peak feature diminishes accompanied by energy red shift. Energy shift is indicated with arrow.

We further conducted a position-dependent study on the photoluminescence spectra surrounding the nanodiamond to gain a deeper understanding of how strain induced by the nanodiamond affects our photoluminescence. Figure 10 reveals that when we are in close proximity to the top of the nanodiamond, the photoluminescence intensity is higher, accompanied by a blue shift in energy, similar to previously observed trends. Notably, as previously observed, the intensity sharply decreases at the top of the diamond, resulting in a distorted peak feature.

To delve into this phenomenon in more detail, we conducted a power dependence study as depicted in Figure 11, focusing on two positions. The first position, far from the bubble and nanodiamond strain, represents the power dependence of the normal heterostructure. The second position, close to the nanodiamond and bubble strain, represents the strained heterostructure. A comparison was then made between the two positions, Point 1 and Point 2 in Figure 11(a).

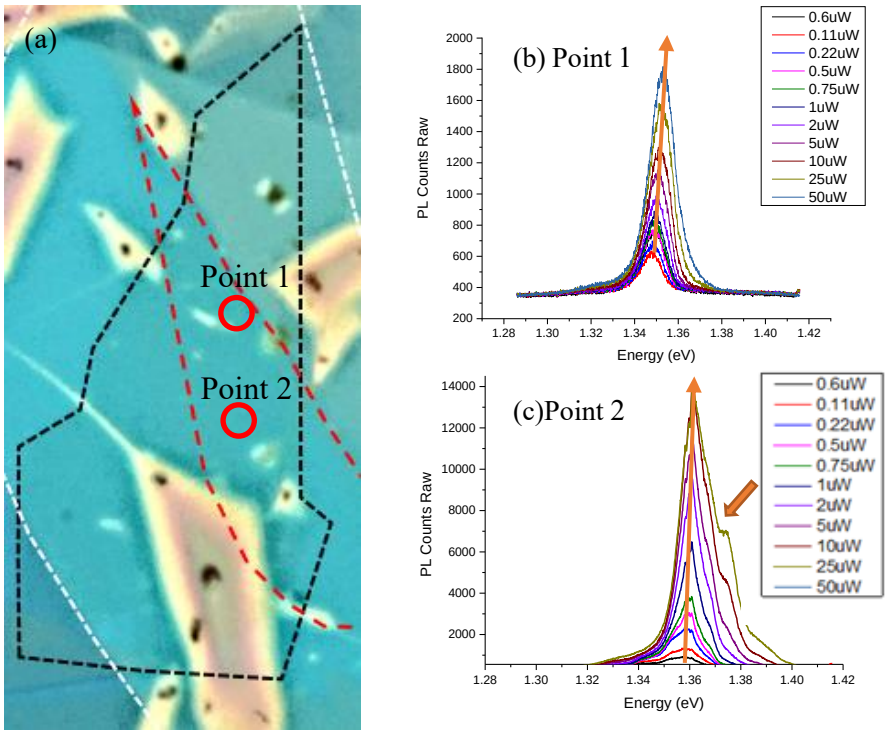

Figure 11. Power dependence of HS off/on the top of bubble starting with nano watt excitation. (a) The optical microscope imaging of sample. The bubbles are shown as the rainbow color with diamond cluster underneath. The strain is large on or nearby these areas. Point 1 is the heterostructure without strain while point 2 is with strain. (b) Optical spectra of point-1 under different illumination power. The PL max count increases with excitation power increase, i.e., the higher power the higher energy peaks. (c) Optical spectra of point-2 under different illumination power. Besides the same phenomenon with (b), we also observed the appearance of the side / shoulder peaks when the power is increased to 10 μW or more.

Figure 11 displays the plotted power dependence curves, where the curve in Figure 11(b) corresponds to the position without bubble strain, indicating an isolated hetero-double layer far from the bubble. Here, we observe a normal power dependence trend, characterized by a blue shift. Conversely, when investigating the heterostructure with bubble or nanodiamond strain (Figure 11(c)), a blue shift is also observed alongside an increase in the intensity of the photoluminescence peak. Interestingly, in addition to the energy blue shift and the heightened photoluminescence peak intensity, a shoulder feature is also observed, providing a direct observation of the strain-induced modulation of photoluminescence.

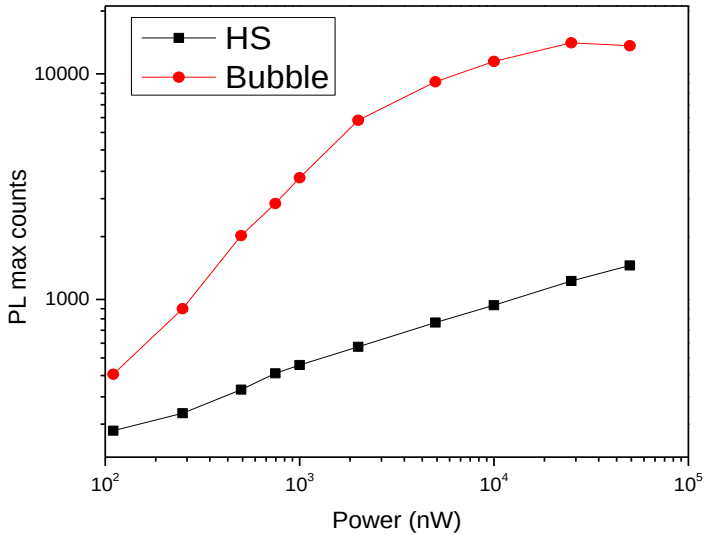

Figure 12. The comparison of the PL max counts of Point-1 and Point-2 under similar illumination power. The plot is under a log scale with PL max count over the excitation power. The red curve is an isolated spot on the hetero bilayer without strain. The black curve is a spot on the hetero bilayer that is close to bubble and nano-diamond. The PL of Point-2 is enhanced by the strain for more than one order. Besides, the PL max count of Point-2 shows a stronger tendency of saturating under increased excitation power.

We assume that this phenomenon is a result of the nanodiamond and bubble strain. Given that this particular spot does not appear to be sandwiched on the edge of the hetero double layer, it

is unlikely to be caused by other photoluminescence effects on the interlayer exciton features.

Therefore, we selected this specific spot for further investigation, conducting an excitation power dependence measurement starting from ～nW, as shown in Figure 12. The peak feature of PL counts from the previous slide was selected and represented on a logarithmic scale. The heterostructure positioned far from bubble strain exhibited a typical trend of increased photoluminescence peak with increasing excitation power, aligning with our expectations.

However, on the spots with bubble strain or near bubble strain, a saturation trend became apparent. As the excitation power increased, the maximum PL count appeared to reach a saturation point. This trend differs significantly from a normal heterostructure without strain. Firstly, the rate of fluorescence intensity growth decreases, deviating from the exponential fluorescence intensity growth observed in normal heterostructures. This suggests the presence of a light-matter interaction different from that in the standard heterostructure.

Chapter 3：1L/2L WSe2 on pillar

In this chapter, we deposited single-layer and double-layer WSe_2 on pillars to achieve more controllable strain and avoid random bubbles (Figure 13). Previously, we deposited the heterostructure on nanodiamond and found the formation of bubbles around the sample, which affected our data analysis. Therefore, we decided to switch to using nanopillars, which were already present on the substrate, as they had consistent lateral positioning and height. This allowed us to further analyze and understand the effects of strain. It is worth noting that this sample differs from the previous one as we are using pillar structures. To enhance the strain, we employed thinner h-BN bottom interlayers. We hope that these nanopillars can induce stronger strain. The cross-sectional overview of the sample deposited on the substrate is shown here. Hopefully, we can obtain better PL results with both sides encapsulated by hexagonal boron nitride (h-BN).

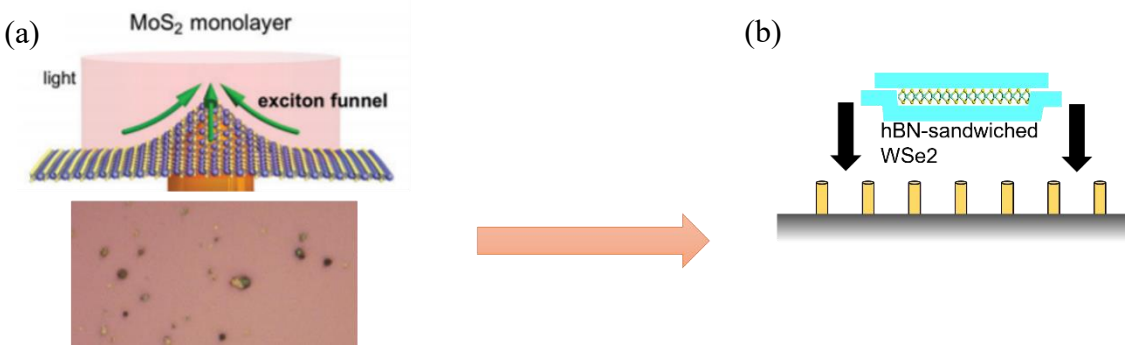

Figure 13. (a) nano-diamond indentation in sample is achieved. With spin-coating technique, big bubbles form during sample fabrication if the cluster of diamond particles underneath has close proximity. Besides, the height of nano-diamond is not uniform and complexes the local strain profile. (b)To avoid bubble strain, more controllable strain can be introduced with periodically spaced pillars.

3.1 fabrication and methods

The fabrication process is relatively complex and requires elaboration. Here, we outline the complete fabrication steps following a mechanical exfoliation using the scotch tape method and microscopic examination in Figure 14. The heterostructure is assembled using a micro manipulator, enabling us to repeatedly pick up and deposit the desired layers for the formation of a van der Waals stack. However, as we aim to deposit the heterostructure onto nano pillars, their height creates a barrier between the sample and the substrate, resulting in a reduced contact surface area. To address this, the temperature is increased to 180 °C in order to melt the plastic film and facilitate the stamping of the sample onto the pillars. Figure 14 (5) is the schematic representation of the assembled structure following the removal of the full phosphorous carbonite film. In Figure 14 (6), we present a side view and top view of our sample shape, respectively. The observed pillars, which are more apparent in the bilayer region, consist of pillar cylinders located beneath the sample surface. The yellow dots represent the nano pillars present on the substrate, while the underlying material is a silicon oxide-silicon substrate. The outlined white dot region represents the bilayer tungsten diselenide. Alongside it, we observe a monolayer tungsten diselenide sample. The presence of the scale bar facilitates the visualization of the sample size, which measures approximately five micrometers.

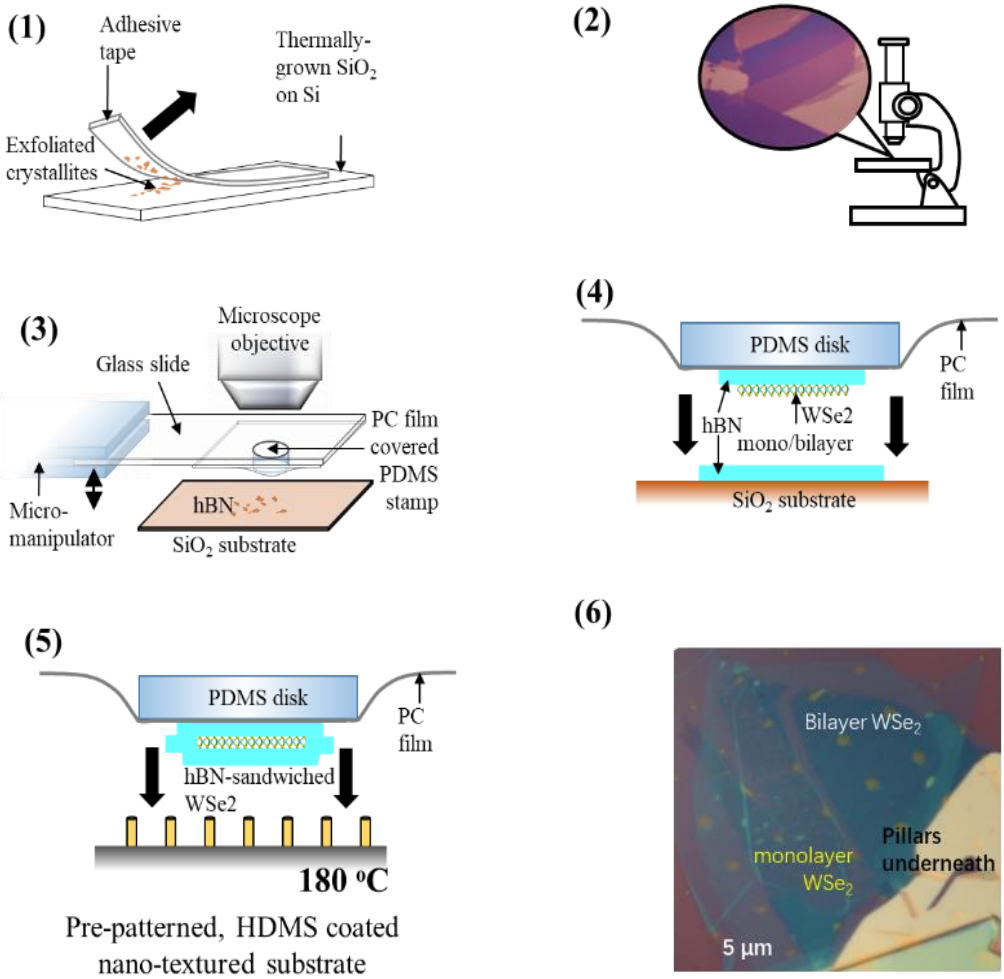

Figure 14. Fabrication steps for locally-strained van der Waals heterostructures on nanopillars. (1) Mechanical exfoliation of WSe2 and hexagonal-boron nitride (h-BN) onto SiO_2/Si, à la "Scotch tape method" (2) Search under microscope for suitable WSe2 mono-/bilayers and thin(~ 10nm) h-BN flakes (3) Use heat-assisted dry transfer method to pick up top h-BN (4) stack of h-BN-sandwiched WSe2 (5) Deposit the heterostructure onto nanopillars by melting down PC film (6) assembled structure after removal of the full phosphorous carbonite film.

3.2 results and discussion

As in previous experiments, we aim to perform photoluminescence measurements on and off the pillars in this study.

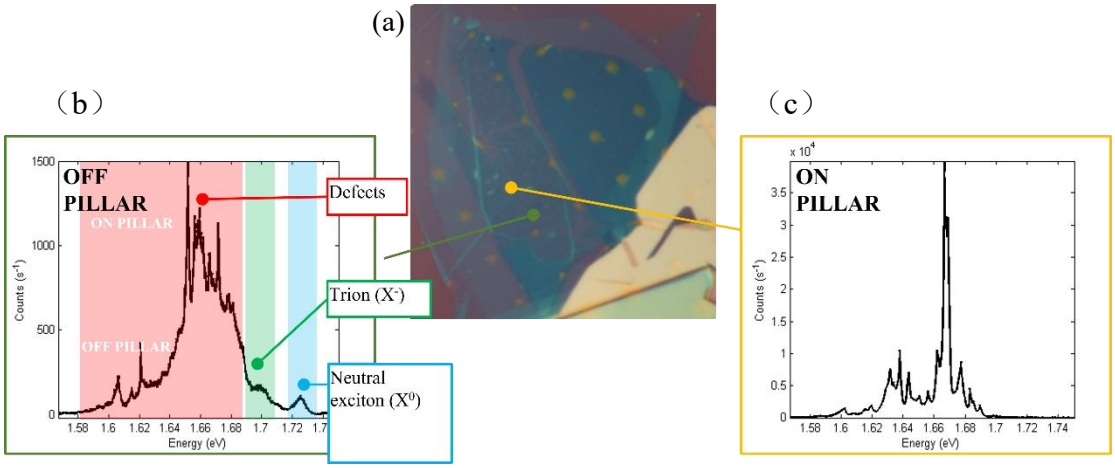

Figure 15. (a) the microscopy imaging of sample, where the pillars are shown as the yellow points array. We measured the spectra on / off pillar, indicated by yellow line and green line respectively. (b) The spectrum at the point off pillar. There is typical monolayer WSe_2 neutral exciton (blue shade) and trion (green shade). PL counts indicate abundant defect information (red region). Spectra shows defect domination. Sharp peak in the defect range (red shade) is very different from previous bubbled samples. (c) the spectrum measured at the point on pillar. The PL max count is enhanced ~20 orders and displays fine feature in the sample, that is different compared to typical WSe_2 monolayer PL signal. The 1L WSe_2 neutral exciton and trion are not drastically enhanced in the pillared spot.

As shown in Figure 15, on the top, we can observe the characteristic photoluminescence of tungsten diselenide (WSe_2), where exciton emissions are located around 721.74 nm. Typically, there are three excitonic features present. One of the weaker excitonic features can be observed at around 1.669 eV. It is noteworthy that the entire PL spectrum is predominantly dominated by this large defect peak, indicating the presence of strong defect emission.

Therefore, we also observed the photoluminescence on the nanowires (Figure 16). Interestingly, we observed a significant enhancement in the photoluminescence intensity on the pillar, reaching up to 20 orders of magnitude higher compared to the off-pillar region. Moreover, the presence of neutral excitons and their behavior in this context is not immediately apparent. Additionally, certain defect peaks on the pillar exhibited enhanced intensities, potentially as a

result of the applied strain. Detailed features may be present in these observations, prompting further analysis.

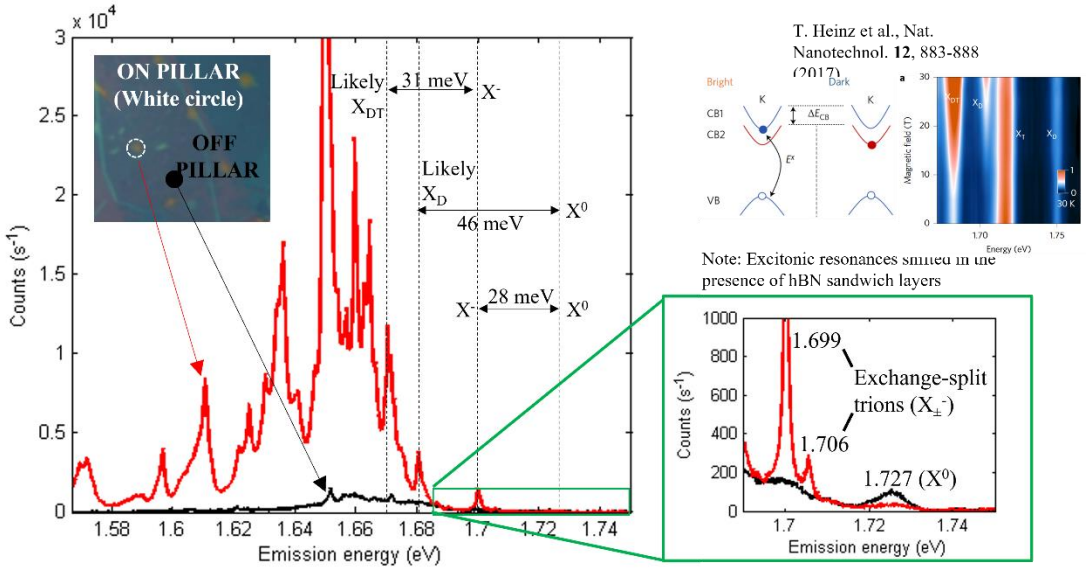

Figure 16. (1) This is the previous plot on and off pillar (combined for comparison). And we can see it is obvious that there is dramatic photoluminescence enhancement on the right for the characteristic part of 1L WSe_2. 2(a) By calculating the energy separation, it is obvious that 2(b) when on pillar, the neutral exciton is weakened, meanwhile the trions is brightened up and exchange-split.

Dark excitons typically involve forbidden, spin-forbidden optical transitions, with a zero in-plane transition dipole moment, making them difficult to detect using conventional far-field optical techniques (due to the traditional difficulties in detecting dark excitons with zero in-plane transition dipole moments). The binding energies of the ionized excitons (or X± three excitons) in monolayer transition metal disulfides can reach several tens of meV, dominating the emission spectra alongside the neutral excitons (X_0) at both low and high temperatures.

Charged excitons, or X± trions, in monolayer transition-metal dichalcogenides have binding energies of several tens of meV. Together with the neutral exciton X_0 they dominate the emission spectrum at low and elevated temperatures.

This perturbation results in the enhancement of dark exciton states, enabling direct observation of light emission from these traditionally inaccessible states. (In a recent study, dark exciton signatures were also observed through coupling to the out-of-plane transition dipole moment using surface plasmon polaritons) [15]. There is also previous paper that reveals when monolayer MoS2 reaches certain amount of strain, the spin order of the conduction band is reversed and the spin forbidden dark exciton gets released and goes below the bright one [34].

Dark excitons are characterized by nominally spin-forbidden optical transitions and possess a zero in-plane transition dipole moment [9], posing challenges for their detection using conventional far-field optical techniques.

Upon closer examination of the significantly intensified peaks, we strongly suspect that the observed brightening corresponds to dark excitons and dark trions. It is supported by our evaluation of the energy separation between the neutral exciton in the dark trion and both the bright trion and dark trion. The measured energy separation matches with the findings reported in a previous study conducted by T. Heinz and Y. Zhou in 2017, which explored the brightening of dark excitons through the application of a magnetic field. Our observed energy separation corresponds to the values reported in their magnetic field measurements under voigt geometry.

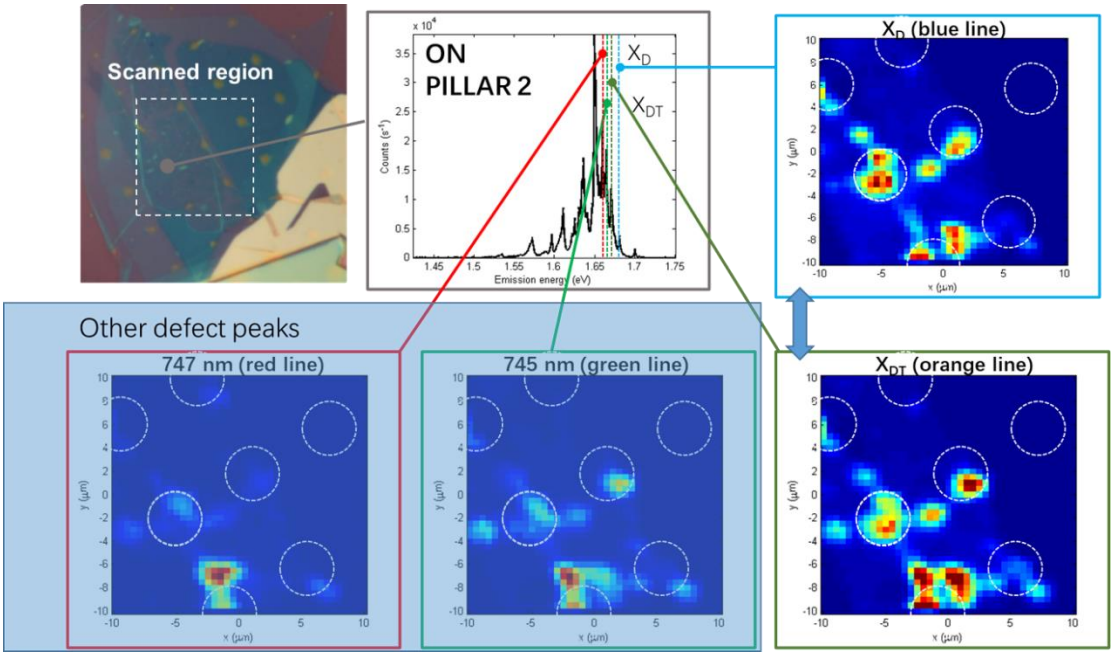

Figure 17. 2D scanning maps of dark exciton and trion, they have similar distribution when on pillars

In conclusion, our findings align with previously reported values for the separation of neutral and dark excitons, as well as the separation of dark and neutral trions. Additionally, bright trions on separations are consistent with prior observations in the literature.

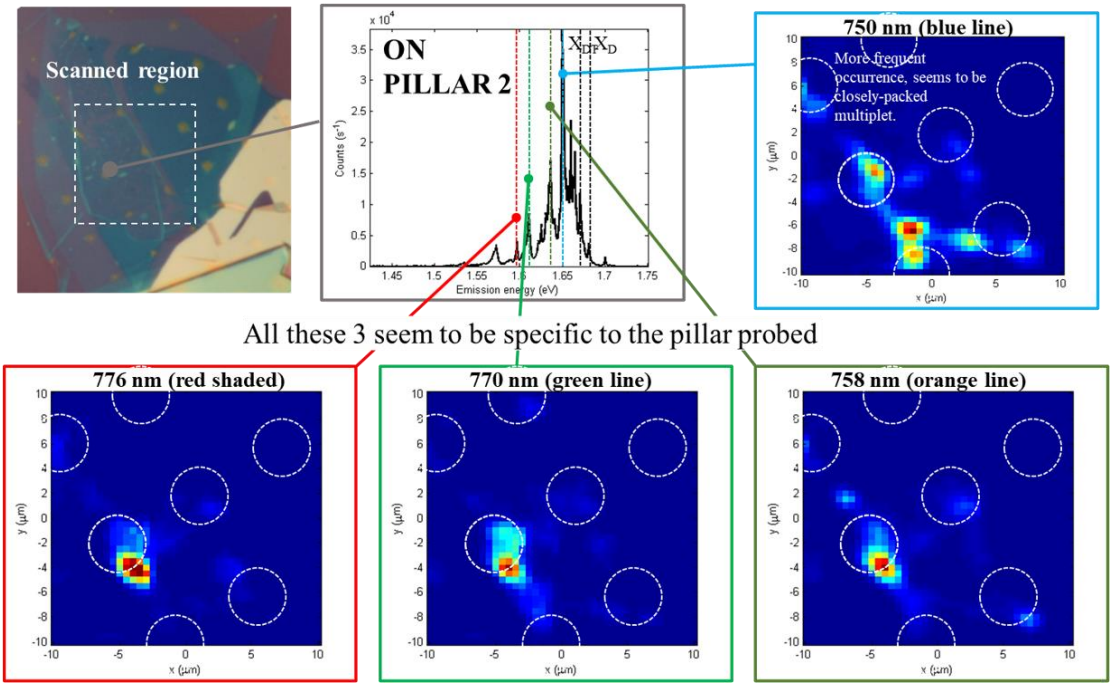

Figure 18. Other less brightened defects in the infrared light spectrum that are on pillars

It is worth mentioning that we possibly observed the brightening of dark exciton states induced by strain. Additionally, we further investigated the peaks corresponding to dark excitons and dark trions. If these phenomena are induced by strain and governed by a specific mechanism that enhances their brightness due to the presence of pillars, we would expect them to appear on multiple pillars. As a result, we obtained spatial maps of both dark excitons and dark trions in Figure 17 and Figure 18. Interestingly, upon examining the pattern observed in the diagram here, we note a resemblance between the distribution of dark trions and dark excitons, both of which appear predominantly on the top of the pillar.

It is highly likely that the dark excitons and their transitions experience a brightening effect under the strain introduced by the pillar. However, further evidence is required to support this hypothesis. Additionally, when examining other bright defect peaks, we observe similar

patterns in their presence near or around the pillar (Figure 17 and Figure 18). It is highly probable that these defects also experience brightening under the pillar-induced strain. We also observe such brightened spots in the vicinity and around the pillars. These brightened spots, however, do not correspond to the pillars, but to smaller nano-scale bubbles. These bubbles, similar to the larger bubbles observed previously, have some ridges that create localized hotspots. Nevertheless, the impact of these nano bubbles on localized brightening is significantly weaker compared to the effect induced by the pillar strain.

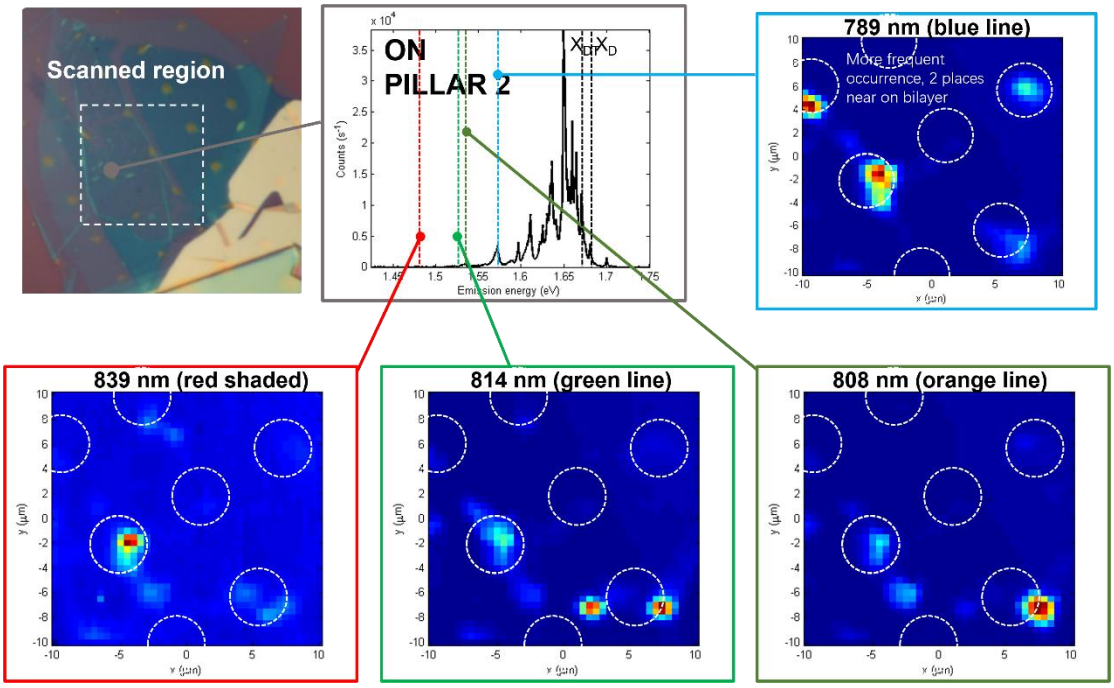

Figure 19. Other interesting peaks from 2L WSe_2, an indirect bandgap semiconductor that does not show characteristic PL signal. However, there is signal here and is not similar to previous reported publications.

It appears that the strain induced by the pillars is still the primary factor in increasing the

brightness of these defect peaks. Additionally, we observe several minor defect peaks at lower energies in Figure 18. These peaks consistently appear in proximity to the pillar regions, which are indicated by white circles outlined here. Interestingly, we also observe a bright spot on the bilayer, which is typically associated with an indirect bandgap material (Figure 19). Therefore, in order to compare the hot spots and pillars, we extracted the photoluminescence spectrum and plotted a waterfall plot. We would say the pillow strain is still dominant in brightening these defect peaks in Figure 20.

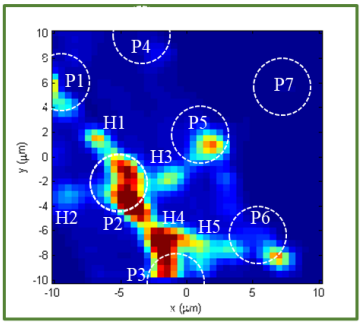

Peaks with more than 3 occurrences (other than X^0, X^-, X_D and X_{DT}):

a. X_{DT} – 5.5 meV
b. X_{DT} – 11 meV
c. 750 nm
d. X_{DT} – 24 meV
e. X_{DT} – 30 meV
f. X_{DT} – 36 meV
g. 770 nm
h. 789 nm

} ~±1 meV uncertainty

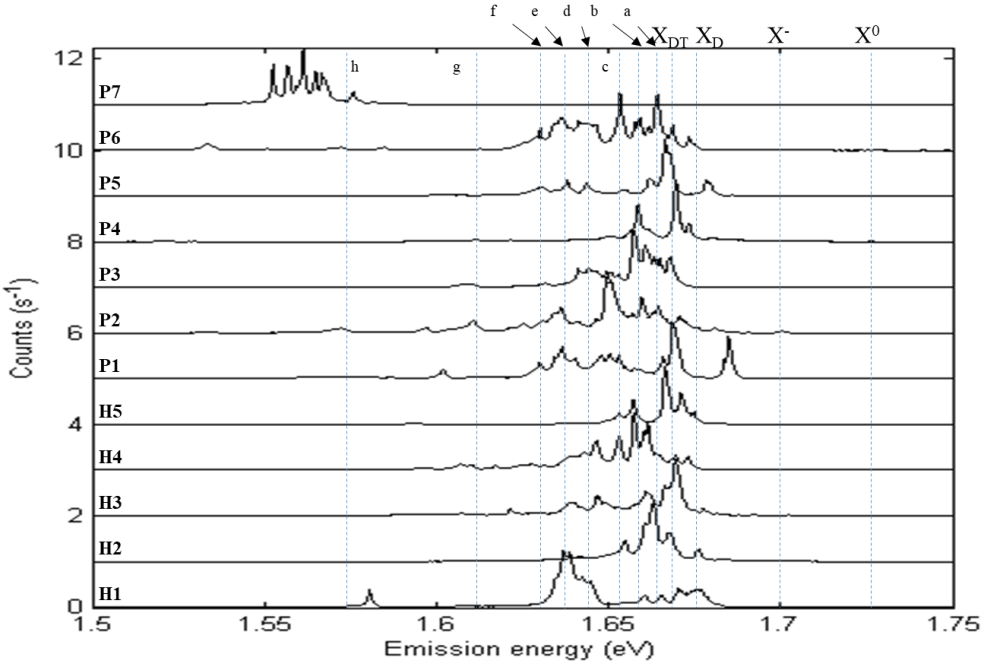

Figure 20. Looking for common features amongst complicated PL information. Compare all 7 pillars and list typical peaks that appear more than 3 times.

Our objective is to determine if the strong PL occurs consistently on multiple pillars, as this would provide stronger evidence. If we observe these occurrences on multiple pillars, we can confidently attribute them to strain-induced effects. Upon comparing and analyzing the data, we observed the presence of peaks such as neutral excitons, dark excitons, dark trions, and other unidentified peaks (referred to as peaks ABCDEFGH). We specifically identified and listed the peaks that occurred more than three times, excluding the characteristic peaks of the material (Figure 20 below). These observed occurrences suggest that these peaks indeed appear repeatedly on pillars or hotspots. Additionally, they exhibit a wide energy distribution, ranging from approximately 1.73 million eV above the neutral exciton energy to around 36 million eV below the dark trion energy.

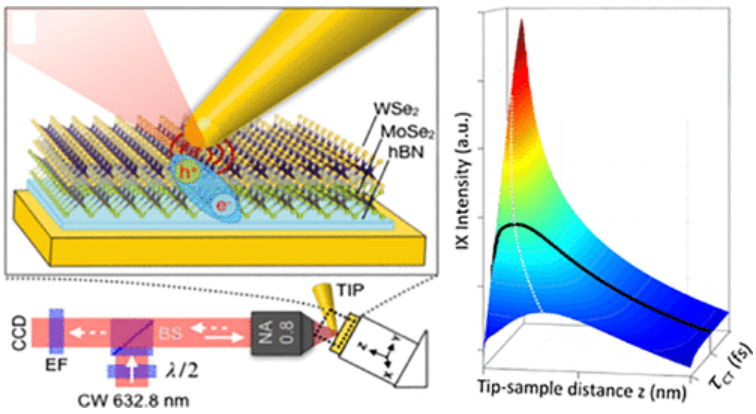

Figure 21. Collaborated work. Nanocavity Clock Spectroscopy: Resolving Competing Exciton Dynamics in $WSe_2/MoSe_2$ Heterobilayers.

However, disentangling the exciton dynamics of these materials is challenging due to the presence of multiple competing processes occurring over a wide range of time scales. A nano-

optical cavity, which can be configured using a plasmonic scanning probe tip, is employed to manipulate the radiative (rad) and non-radiative (nrad) relaxation of intra- and interlayer excitons. The nanocavity clock spectroscopy approach can be applied to a broad range of excitonic systems that exhibit multiple competitive decay pathways.

We also observed defects at 770 nanometers and 790 nanometers. These defects are particularly relevant for infrared region solar cell applications. In collaboration with Professor Raschke, we employed a sophisticated optical setup to characterize the populations of dark and bright states. The resulting findings are published in a separate paper[35]. In this study, I'm in charge of the preparation of a WSe2/MoSe2/h-BN heterostructure on a gold substrate. Additionally, similar work was conducted in the same year but focused on electrically driven systems. Furthermore, by introducing strain, they observed deterministic single photon emitters in the van der Waals heterostructure. Therefore, the findings from our work suggest that our observed phenomenon can potentially serve as a promising candidate for a deterministic single photon emitter, consisting of quantum dot-like particles that hold relevance in quantum computation.

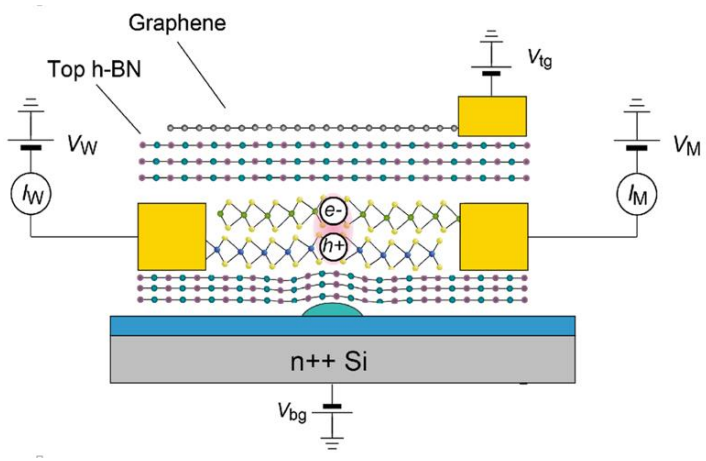

Figure 22. Finite scheme for future study

Chapter 4. Summary and outlook

Throughout my master thesis, I primarily focused on fabricating and characterizing locally strained WSe_2 and $MoSe_2$ materials, as well as investigating their impact on the optical properties. Two methods were employed: one involved particles for creating nano indentations in the material, while the other utilized strategically spaced pillars to induce strain in a periodic and controllable manner. This approach minimized the formation of undesired bubbles commonly encountered in earlier experiments. Both samples were deposited onto the nano diamond, where the presence of both the nano diamond and introduced strain from the bubbles resulted in altered photoluminescence characteristics. Furthermore, distinct power dependence of excitation was observed on the pristine structure without strain, as well as on the structure containing bubble-induced strain. Consequently, both samples exhibited a notable spectral shift towards higher energy, indicative of strain-induced effects.

Additionally, we accurately deposited the WSe_2 monolayer and bilayer onto pillars with a lateral precision of one to two micrometers. Furthermore, we conducted characterization of the photoluminescence both with and without strain. The strained photoluminescence from the pillars exhibited higher counts per second and significantly enhanced brightness of excitons. We also collaborated with other researchers using a similar experimental setup.

Moving forward, in our future work and research outlook, we can explore the application of electrically driven, individually contacted layers and utilize gates to manipulate carrier density through electric field tuning. Additionally, we can potentially enhance the optical quality of our

samples by implementing improved hexagonal boron nitride encapsulation. Furthermore, it is intriguing to explore potential research directions and applications in this field. Notably, we have previously observed the use of strain to enhance the tuning capabilities of our defects. Additionally, we have possibly observed strain-induced brightening of dark excitonic states in WSe_2, which presents the possibility of utilizing it as a potential quantum dot candidate for quantum computations. Furthermore, by utilizing heterostructures composed of different stacked materials, we can leverage strain engineering to delve deeper into the development of advanced electronic devices.

The transition from direct to indirect bandgap is observed in various semiconducting TMD materials, such as WSe_2, when transitioning from single-layer to bilayer structures. Monolayers have been extensively studied for a range of applications, including chemical sensing and quantum emission. However, WSe_2 bilayer TMDs are highly desirable for various applications, notably in piezoelectric devices, valleytronics, photodetectors, and transistors, owing to their enhanced stability and superior carrier mobility. Furthermore, bilayer systems offer an additional degree of freedom: the twist angle.

Acknowledgement

I would like to express my gratitude to the dedicated research team at the Xu Lab. I extend special thanks to Professor Xiaodong Xu for his invaluable support throughout my years as a graduate student. Additionally, I am grateful to Gen, Kyle, Pasqual, Essence, Dimitry, and Colin for their assistance and collaboration in our projects. I am also grateful to other professors and labs for helpful discussion and for providing the pillar substrates. I would like to express my appreciation to Prof. Raschke Lab for providing nano diamond and collaborating with Dr. Molly May, a brilliant researcher who contributed significantly to the optical characterization of our work.

References:

[1] Novoselov, K. S. et al. Electric field effect in atomically thin carbon films. Science 306, 666–669 (2004).

[2] Novoselov, K. S. et al. Two-dimensional atomic crystals. Proc. Natl Acad. Sci. USA 102, 10451–10453 (2005).

[3] K. S. Novoselov, D. Jiang, F. Schedin, T. J. Booth, V. V. Khotkevich, S. V. Morozov, and A. K. Geim. Two-dimensional atomic crystals. Proc. Natl Acad. Sci. USA 102, 10451 (2005).

[4] Kin Fai Mak, Changgu Lee, James Hone, Jie Shan, and Tony F. Heinz, Atomically Thin MoS_2: A New Direct-Gap Semiconductor. Phys. Rev. Lett. 105, 136805 (2010).

[5] Radisavljevic, B., Radenovic, A., Brivio, J. et al. Single-layer MoS2 transistors. Nature Nanotechnology 6, 147–150 (2011).

[6] Di Xiao, Gui-Bin Liu, Wanxiang Feng, Xiaodong Xu, and Wang Yao. Coupled Spin and Valley Physics in Monolayers of MoS2 and Other Group-VI Dichalcogenides. Phys. Rev. Lett. 108, 196802 (2012).

[7] Lopez-Sanchez, O., Lembke, D., Kayci, M. et al. Ultrasensitive photodetectors based on monolayer MoS2. Nature Nanotechnology 8, 497–501 (2013).

[8] A.K. Geim, I. V. Grigorieva. Van der Waals heterostructures. Nature 499, 419–425 (2013).

[9] Rivera, P., Schaibley, J., Jones, A. *et al.* Observation of long-lived interlayer excitons in monolayer $MoSe_2$–WSe_2 heterostructures. Nature Communications 6, 6242 (2015).

[10] Clark, G. et al. Single defect light-emitting diode in a van der Waals heterostructure. Nano Letters 16, 3944-3948 (2016).

[11] Kumar, S., Kaczmarczyk, A., Gerardot, B. D. Strain-induced Spatial and Spectral Isolation Of Quantum Emitters In Mono- And Bilayer Wse2. Nano Letters, 11, 7567-7573 (2015).

[12] He, YM., Clark, G., Schaibley, J. et al. Single quantum emitters in monolayer semiconductors. Nature Nanotechnology 10, 497–502 (2015).

[13] Matin Amani et al, Near-unity photoluminescence quantum yield in MoS2. Science 350, 1065-1068 (2015).

[14] He, YM., Clark, G., Schaibley, J. et al. Single quantum emitters in monolayer semiconductors. Nature Nanotechnology 10, 497–502 (2015).

[15] Ermin Malic, Malte Selig, Maja Feierabend, Samuel Brem, Dominik Christiansen, Florian Wendler, Andreas Knorr, and Gunnar Berghäuser. Dark excitons in transition metal dichalcogenides. Phys. Rev. Materials 2, 014002 (2018).

[16] Zhang, XX., Cao, T., Lu, Z. et al. Magnetic brightening and control of dark excitons in monolayer WSe2. Nature Nanotechnology 12, 883–888 (2017).

[17] Geim, A. K. & Grigorieva, I. V. Van der Waals heterostructures. Nature 499, 419-425 (2013).

[18] Novoselov, K. S., Mishchenko, A., Carvalho, A. & Castro Neto, A. H. 2D materials and van der Waals heterostructures. Science 353, 9439 (2016).

[19] Mak, K. F. & Shan, J. Photonics and optoelectronics of 2D semiconductor transition metal dichalcogenides. Nature Photonics 10, 216-226 (2016).

[20] Rafael Roldán, Andrés Castellanos-Gomez, Emmanuele Cappelluti, Francisco Guinea. Strain engineering in semiconducting two-dimensional crystals. *J. Phys.: Condens. Matter* 27 313201 (2015).

[21] Shikai Deng, Anirudha V. Sumant, Vikas Berry. Strain engineering in two-dimensional nanomaterials beyond graphene. Nano Today, Volume 22, 14-35 (2018).

[22] Manzeli, S., Allain, A., Ghadimi, A., Kis, A. Piezoresistivity and Strain-induced Band Gap Tuning In Atomically Thin MoS_2. Nano Letters, 8, 5330-5335 (2015).

[23] Hui, Y. Y., et al., Exceptional Tunability Of Band Energy In a Compressively Strained Trilayer MoS_2 Sheet. ACS Nano, 8, 7126-7131 (2013).

[24] Yang, R., Lee, J., Ghosh, S., Hall, M. B., Sankaran, R. M., Zorman, C. A., … & Feng, P. X. Tuning Optical Signatures of Single- and Few-layer Mos2 By Blown-bubble Bulge Straining Up To Fracture. Nano Letters, 8, 4568-4575 (2017).

[25] Britnell, L. et al. Strong light–matter interactions in heterostructures of atomically thin films. Science 340, 1311–1314 (2013).

[26] Dean, C. R. et al. Boron nitride substrates for high-quality graphene electronics. Nature nanotechnology 5, 722-726 (2010).

[27] Wang, L. et al. One-dimensional electrical contact to a two-dimensional material. Science 342, 614-617 (2013).

[28] Kin Fai Mak, Changgu Lee, James Hone, Jie Shan, and Tony F. Heinz. Atomically Thin MoS2: A New Direct-Gap Semiconductor. Phys. Rev. Lett. 105, 136805 (2010).

[29] Splendiani, A., et al., Emerging Photoluminescence In Monolayer Mos2. Nano Letters, 4, 1271-1275 (2010).

[30] Shikai Deng, Anirudha V. Sumant, and Vikas Berry*, Strain Engineering in Two-Dimensional Nanomaterials Beyond Graphene. Nanotoday 22, 14-35 (2018).

[31] Zhaohe Dai, Luqi Liu, and Zhong Zhang, Strain Engineering of 2D Materials: Issues and Opportunities at the Interface. Advanced Materials 31, 1805417 (2019).

[32] P. San-Jose, V. Parente, F. Guinea, R. Roldán and E. Prada, Inverse Funnel Effect of Excitons in Strained Black Phosphorus. Phys. Rev. X 6, 031046 (2016).

[33] Dependence of band structure and exciton properties of encapsulated WSe2 monolayers on the hBN-layer thickness.Iann C. Gerber and Xavier Marie.Phys. Rev. B 98, 245126 (2018)

[34] Strain-induced dark exciton generation in rippled monolayer MoS2 Su Yeon g Lee, Won Seok Yun and J. D. Lee. Phys. Chem. Chem. Phys., 25, 9894-9900(2023)

[35] Molly A. May, Tao Jiang, Chenfeng Du, Kyoung-Duck Park, Xiaodong Xu, Alexey Belyanin*, and Markus B. Raschke*. Nanocavity Clock Spectroscopy: Resolving Competing Exciton Dynamics in WSe2/MoSe2 Heterobilayers, Nano Letters 21, 522–528 (2021)

[36] Thomas Mueller, Ermin Malic. Exciton physics and device application of two-dimensional transition metal dichalcogenide semiconductors. Nature 29, 0074 (2018)